(Received 10 October 2024, Accepted 16 December 2024, Scheduled 19 December 2024)

Confocal Microscopy with Optimized Excitation and Emission Wavelength for Ultradeep and Multi-Channel Bioimaging

Tianxiang Wu[1], Weihang Geng[1], Yuhuang Zhang[1], Qiming Xia[2], Mingxi Zhang[3], Jin Li[4], Menglu Chen[5, 6], Wang Xi[7], Shiyi Peng[1], Zhe Feng[1], and Jun Qian[1, *]

[1] *State Key Laboratory of Extreme Photonics and Instrumentation Centre for Optical and Electromagnetic Research, College of Optical Science and Engineering International Research Center for Advanced Photonics, Zhejiang University, Hangzhou 310058, China*
[2] *Department of General Surgery, Sir Run Run Shaw Hospital, Zhejiang University School of Medicine, Hangzhou 310016, China*
[3] *State Key Laboratory of Advanced Technology for Materials Synthesis and Processing Wuhan University of Technology, Wuhan 430070, China*
[4] *State Key Laboratory Breeding Base of Green-Chemical Synthesis Technology Institute of Green Petroleum Processing and Light Hydrocarbon, College of Chemical Engineering Zhejiang University of Technology, Hangzhou 310014, China*
[5] *School of Optics and Photonics, Beijing Institute of Technology, Beijing, 100081, China*
[6] *Westlake Institute for Optoelectronics, Fuyang, Hangzhou 311421, China*
[7] *Interdisciplinary Institute of Neuroscience and Technology (ZIINT) the Second Affiliated Hospital, School of Medicine, Zhejiang University, Hangzhou 310020 China*

ABSTRACT: The second near-infrared region (NIR-II, 900–1880 nm) spectral window has garnered significant attention in bioimaging due to its moderate light absorption, diminished photon scattering and reduced autofluorescence. Exploiting NIR-II fluorescence, confocal microscopy has achieved deep *in vivo* imaging. In this study, we have identified that the fluorescence with wavelength beyond 1400 nm offers superior imaging quality for NIR-II confocal microscopy, irrespective of the laser excitation source being continuous-wave or pulsed. Furthermore, leveraging the multiphoton excitation capabilities of femtosecond laser, we have successfully integrated multiphoton excited visible fluorescence channels into the NIR-II fluorescence confocal microscopic system. We have successfully employed this novel system to acquire up to six distinct fluorescence microscopic imaging channels with negligible cross-channel interference, as well as multi-channel and large-depth in vivo observation of mouse brain and kidney.

1. INTRODUCTION

Fluorescence imaging has become a cornerstone in biomedical research, renowned for its exceptional sensitivity, non-invasive nature, and absence of ionizing radiation risks. This modality allows for the visualization of biological processes with high spatial and temporal resolution, making it an indispensable tool for studying biological dynamics and molecular interactions [1]. Fluorescence confocal microscopy is a prominent technique that have been extensively employed in the realm of biomedical imaging [2, 3]. Confocal microscopic imaging employs a pinhole to eliminate out-of-focus light, capturing only the signals from the focal point. It generates high-resolution images through point-by-point scanning and obtains three-dimensional (3D) images via reconstruction, enabling precise biological visualization. It offers the advantage of optical sectioning, which enables the acquisition of high-resolution images from thick biological samples. However, the penetration of confocal microscopic imaging into biological tissues is inherently constrained by the photon scattering and light absorption of biological tissues. Previous studies have demonstrated that longer wavelengths light exhibits reduced scattering within tissues, thereby enabling near-infrared (NIR) fluorescence imaging to achieve larger depths than visible fluorescence imaging [4]. The second near-infrared window [4, 5], designated as NIR-II, encompasses the spectral range of 900 to 1880 nm. This particular range is distinguished by its diminished photon scattering and favorable light absorption of water, which lead to a notable improvement in the signal-to-background ratio (SBR), thereby enhancing the clarity and depth of fluorescence imaging [6]. Exploiting NIR-II fluorescence, confocal microscopy can achieve deep and high-resolution in vivo observation [7–13].

In recent scholarly endeavors, the domain of NIR-II confocal microscopy has concentrated on extending the excitation and emission wavelengths to harness the potential for enhanced imaging penetration. In 2019, our research group accomplished mouse cerebral vascular imaging at a depth of 900 µm by utilizing a 793 nm continuous-wave (CW) laser to excite indocyanine green (ICG), with fluorescence detection beyond 1000 nm [11]. Subsequently, in 2021, Xu's group extended the depth of cranial cerebral vascular imaging to 1.7 mm using a 1310 nm CW laser to excite quantum dots, coupled with the single-photon avalanche diode (SPAD) or superconducting nanowire single-photon detector (SNSPD) technology

* Corresponding author: Jun Qian (qianjun@zju.edu.cn).

for detecting fluorescence emissions above 1600 nm [14]. In 2022, Dai's group further advanced the field by achieving 1 mm depth craniotomy brain imaging in mice, employing a 1650 nm CW excitation source to excite quantum dots, with fluorescence emission detected over 1700 nm using SNSPD [15]. These milestones highlighted the continuous refinement in imaging depth and spatial resolution, attributable to the judicious utilization of longer wavelength excitation and emission of fluorescent probes. However, the pursuit of imaging depths in NIR-II confocal microscopy should not be solely directed towards the extension into longer wavelength excitation and emission. The existing body of research is notably limited in its exploration of imaging quality across diverse fluorescence wavelengths in NIR-II confocal microscopy, particularly when utilizing identical fluorescent probes and maintaining constant conditions, such as the excitation light source. Our previous research has indicated that a moderate level of light absorption by tissues can augment the fraction of ballistic photons within the detected signal, thereby enhancing the SBR of the imaging. This phenomenon is particularly pronounced within the spectral window of 1400–1500 nm, where water exhibits appropriate light absorption, thus enhancing the imaging contrast [6, 16]. Optimizing the imaging outcome through wavelength adjustment of the detected fluorescence presents a compelling area of inquiry. By tuning the wavelength of fluorescence detected by the system, the imaging quality can be significantly modulated. This is particularly pertinent given that many hardware components of confocal systems are not readily amenable to modification. Our prior studies have revealed that employing a detection window beyond 1400 nm, specifically utilizing a 1400 nm long-pass filter, yields superior SBR and enhanced imaging depths compared to other similar NIR-II sub-windows in macroscopic and wide-field microscopic imaging [6, 17]. However, the findings of prior investigations have been predicated on the imaging using two-dimensional (2D) array detectors. It is imperative to conduct further research to ascertain the applicability and validity of these findings when transitioning to point-excitation and point-detection imaging modalities such as NIR-II fluorescence confocal microscopy.

The imaging depth is a critical parameter in confocal microscopy, however, the number of imaged channels is equally significant. Recent advancements have focused on incorporating fluorescence lifetime measurements into confocal microscopy, thereby enhancing the dimensionality of the imaging channels [13]. Furthermore, a substantial body of research has been dedicated to the development of multi-channel imaging techniques. These studies have leveraged the unique fluorescence emission spectra of distinct probes by employing multiple spectral windows, which allows for the simultaneous acquisition of multiple channels [17–23]. The majority of these investigations have opted for CW laser excitation as a means to achieve this multi-channel capability, as documented in several literatures [15, 23, 25]. When a femtosecond laser is used for excitation, it is possible to introduce multiphoton fluorescence into the microscopic system at the same time. Multiphoton fluorescence microscopy is based on the nonlinear optical effect of multiphoton absorption. This technique circumvents the need for a pinhole to reject out-of-focus signals, opting instead for a high-energy pulsed laser that restricts excitation to the focal point. Multiphoton fluorescence microscopy has been extensively applied across the biomedical field [24, 25], significantly enhancing our ability to study complex biological processes and structures. Nevertheless, multiphoton fluorescence microscopic systems often exhibit compatibility challenges with confocal microscopic channels due to their distinct excitation light requirements, thereby precluding simultaneous imaging capabilities.

In this work, we have revealed that employing a detection window beyond 1400 nm, fluorescence bioimaging yields superior SBRs and enhanced depths compared to that in other NIR-II sub-windows. This is observed even when the fluorescent probes exhibit reduced brightness within this spectral range. This work marks the first instance of its unique advantages being identified within the context of NIR-II confocal microscopy. Simultaneously, to enhance the multi-channel imaging capabilities of the NIR-II microscopy and to mitigate the compatibility issues between multiphoton fluorescence and NIR-II fluorescence confocal microscopy, the integration of a 930 nm femtosecond laser into the microscopic system was implemented. The 930 nm pulsed laser was instrumental in the construction of a multi-channel microscopic imaging system, as it facilitated the integration of two-photon fluorescence channels without compromising the integrity of NIR-II fluorescence channels. This integration significantly expanded the imaging channel capacity of the microscope. Thus, we synergistically combined two-photon fluorescence and NIR-II fluorescence confocal channels, thereby enabling up to six distinct imaging channels. Concurrently, we conducted *in vivo* microscopic imaging of the mouse brain and kidney, achieving three-channel imaging of neurons, glial cells and blood vessels in brain tissue at depths exceeding 200 μm, as well as dual-channel imaging of glomeruli and tubules in the kidney at depths over 220 μm. This technological advancement holds substantial promise for applications in the investigation of physiological processes and the intricate interactions within living organisms.

2. RESULT AND DISCUSSION

2.1. Spectral Window beyond 1400 nm in NIR-II Fluorescence Confocal Microscopy for Enhanced Imaging Quality

In the investigation of deep-tissue mouse brain imaging employing NIR-II fluorescence confocal microscopy, a series of long-pass filters with varying cutoff wavelengths were strategically utilized to selectively capture distinct fluorescence emission spectra. The fluorescent probes employed in this study were PbS/CdS quantum dots, characterized by a peak emission wavelength of 1450 nm (referred to as 1450 QDs). Owing to the pronounced absorption peak of water at 1450 nm, the emission spectrum of the 1450 QDs exhibits a corresponding dip at this wavelength, as depicted in Figure 1(a).

The intensity acquisition capabilities of the detector, contingent upon the deployment of distinct long-pass filters, are illustrated in Figure 1(b). Specifically, the intensity harvested with the 1300 nm long-pass filter is approximately 1.5-fold and 2.3-

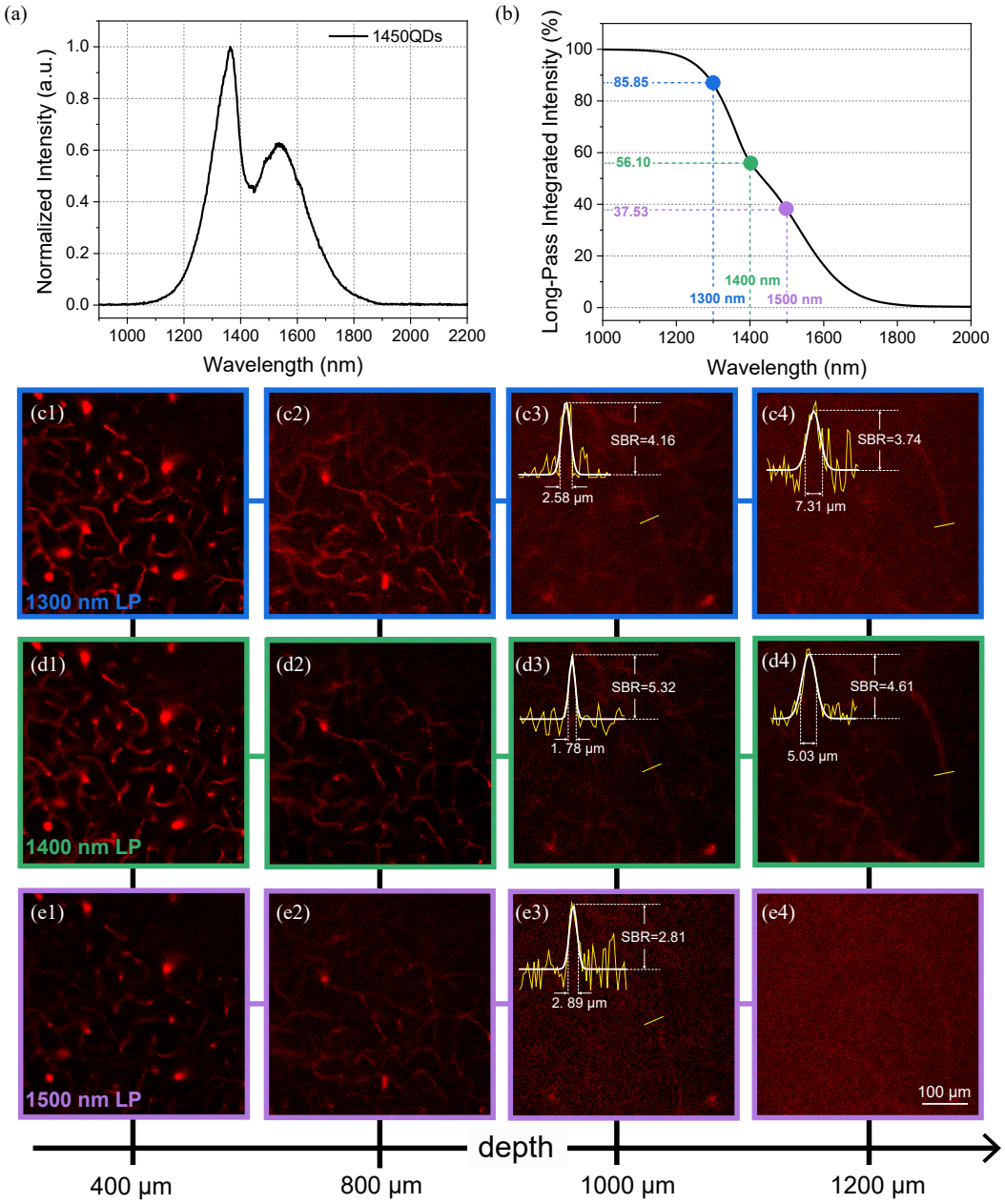

FIGURE 1. *In Vivo* NIR-II confocal microscopic imaging of cerebral vessels in mice utilizing 1177 nm CW laser excitation. (a) Fluorescence emission spectrum of 1450 QDs. (b) The integrated fluorescence intensity spectrum of 1450 QDs as collected by LP filters with varying cutoff wavelengths within the 1000–2000 nm range. The relative integrated fluorescence intensities captured by the 1300 nm, 1400 nm, and 1500 nm LP filters are indicated. (c1)–(c4) Images at varying depths employing the 1300 nm LP filter, achieving a resolution of 7.31 μm blood vessels at a depth of 1200 μm with a SBR of 3.74. (d1)–(d4) Images at varying depths using the 1400 nm LP filter, resolving a 5.03 μm vessel at 1200 μm depth with an SBR of 4.61. (e1)–(e4) Images at varying depths with the 1500 nm LP filter, failed to resolve vessels at the 1200 μm depth; however, at 1000 μm depth, a 2.89 μm vessel was successfully imaged.

fold that of the 1400 nm and 1500 nm long-pass filters, respectively. From the perspective of intensity collection efficiency, one might anticipate that the image quality associated with the 1400 nm (1400 LP) and 1500 nm (1500 LP) long-pass filters would be inferior to that of the 1300 nm (1300 LP) long-pass filter. However, contrary to these expectations, empirical findings reveal that the imaging outcomes procured with the 1400 LP filter surpass those of the 1500 LP filter in terms of imaging depth and outperform the 1300 LP filter in resolution and SBR.

As delineated in Figures 1(c)–(e), the maximal imaging depth attainable under the excitation of an 1177 nm CW laser was 1.2 mm. At this depth, the vascular structures were discernible with a SBR of 3.74 when employing the 1300 nm LP filter. In contrast, the SBR improved to 4.61 with the utilization of the 1400 nm LP filter. Conversely, the 1500 nm LP filter failed to resolve the vessels at the 1.2 mm depth, likely attributable to diminished signal intensity. Upon reducing the imaging depth

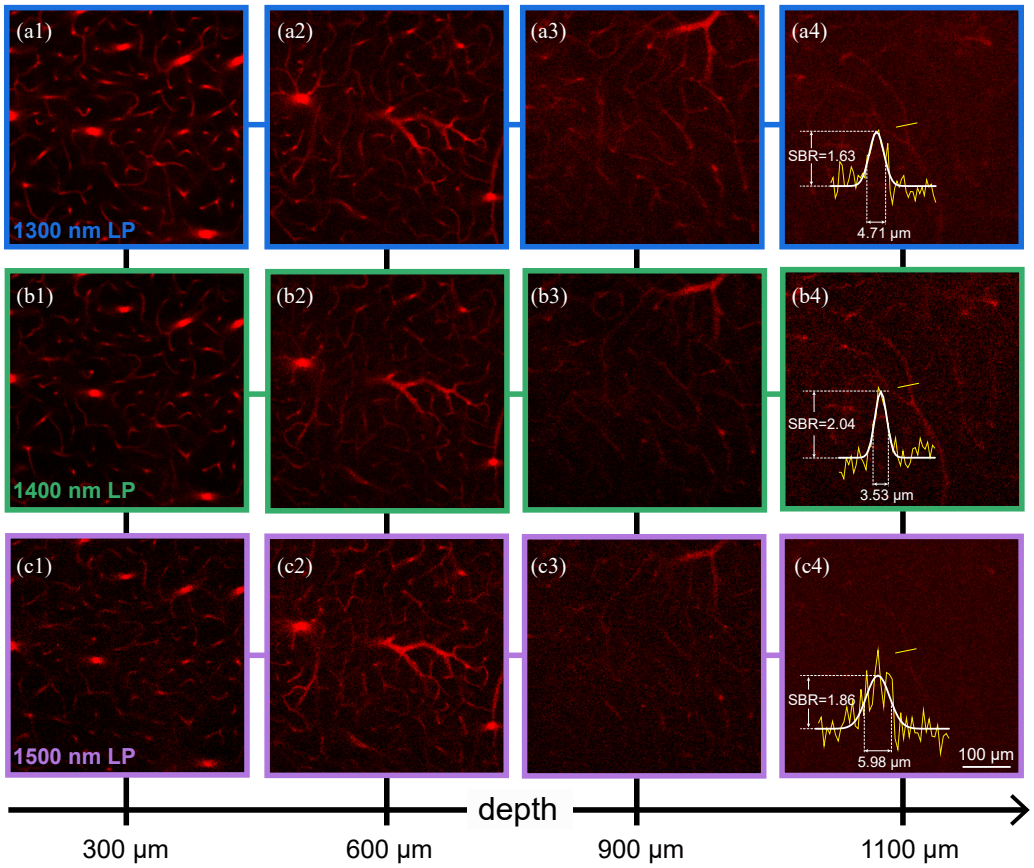

FIGURE 2. *In Vivo* NIR-II confocal microscopic imaging of cerebral vessels in mice utilizing 930 nm femtosecond laser excitation. (a1)–(a4) Images at various depths using a 1300 nm LP filter, demonstrating the capability to resolve a 4.71 μm vessel at a depth of 1100 μm with a SBR of 1.63. (b1)–(b4) Images at various depths with a 1400 nm LP filter, achieving resolution of a 3.53 μm vessel at 1100 μm depth with an SBR of 2.04. (c1)–(c4) Images at various depths employing a 1500 nm LP filter, resolving a 5.98 μm vessel at 1100 μm depth with an SBR of 1.86.

to 1 mm, the 1500 nm LP filter became capable of resolving the vascular structures.

In the aforementioned experimental outcomes, the characteristics of the excitation light source remained constant; the variable manipulation was the detected fluorescence wavelength, which was selectively altered by adjusting the filter settings within the system. Upon transitioning to a 930 nm femtosecond laser for excitation, the aforementioned findings remained valid. Figure 2 presents confocal images of mouse cerebral vessels acquired using a 930 nm femtosecond laser excitation. The border colors of the images correspond to different detection filters. Specifically, Figure 2(a) corresponds to the 1300 LP, Figure 2(b) to the 1400 LP, and Figure 2(c) to the 1500 LP. As depicted in Figure 2(b4), the maximal depth achievable for brain imaging with the 930 nm excitation was approximately 1.1 mm. This depth was somewhat reduced compared to that attained with the 1177 nm excitation, which can be attributed to the increased scattering of the 930 nm light within the tissue. As illustrated in Figures 2(a4)/(b4)/(c4), at a depth of 1.1 mm, a blood vessel with a diameter of 4.71 μm was discernible with an SBR of 1.63 when utilizing the 1300LP filter. In contrast, the application of the 1500 LP filter yielded an image with a superior SBR of 1.86; however, this came at the expense of reduced resolution, with the vessel appearing with a diameter of 5.98 μm. Utilizing the 1400 LP filter, the imaging resulted in an enhanced SBR of 2.04 coupled with a higher resolution of 3.53 μm for the vessels.

Utilizing the Monte Carlo method, we simulated the fluorescence collection process of the confocal system to underscore the influence of the detection wavelength selection on the ultimate quality of fluorescence confocal imaging. The simulation methodology and associated parameter settings are comprehensively described in the Supplementary Information. The simulation outcomes reveal extreme values in fluorescence collection efficiency at wavelengths of 1410 nm, 1500 nm,1880 nm, and 2150 nm, as depicted in Figure S2(e) in Supplementary Information. The confocal effective collection spectrum peaking around NIR-IIx (1400–1500 nm) provides a robust theoretical foundation for the enhanced imaging performance of the 1400LP images compared to the 1300LP and 1500LP ones.

2.2. Multi-Channel Microscopic Imaging in the Visible-to-NIR-II Region Enabled by 930 nm Femtosecond Laser Excitation

A 930 nm femtosecond laser was selected due to its versatility as an excitation light source, suitable for both multiphoton fluorescence and NIR-II fluorescence confocal microscopic systems, thereby facilitating *in vivo* multi-channel imaging at

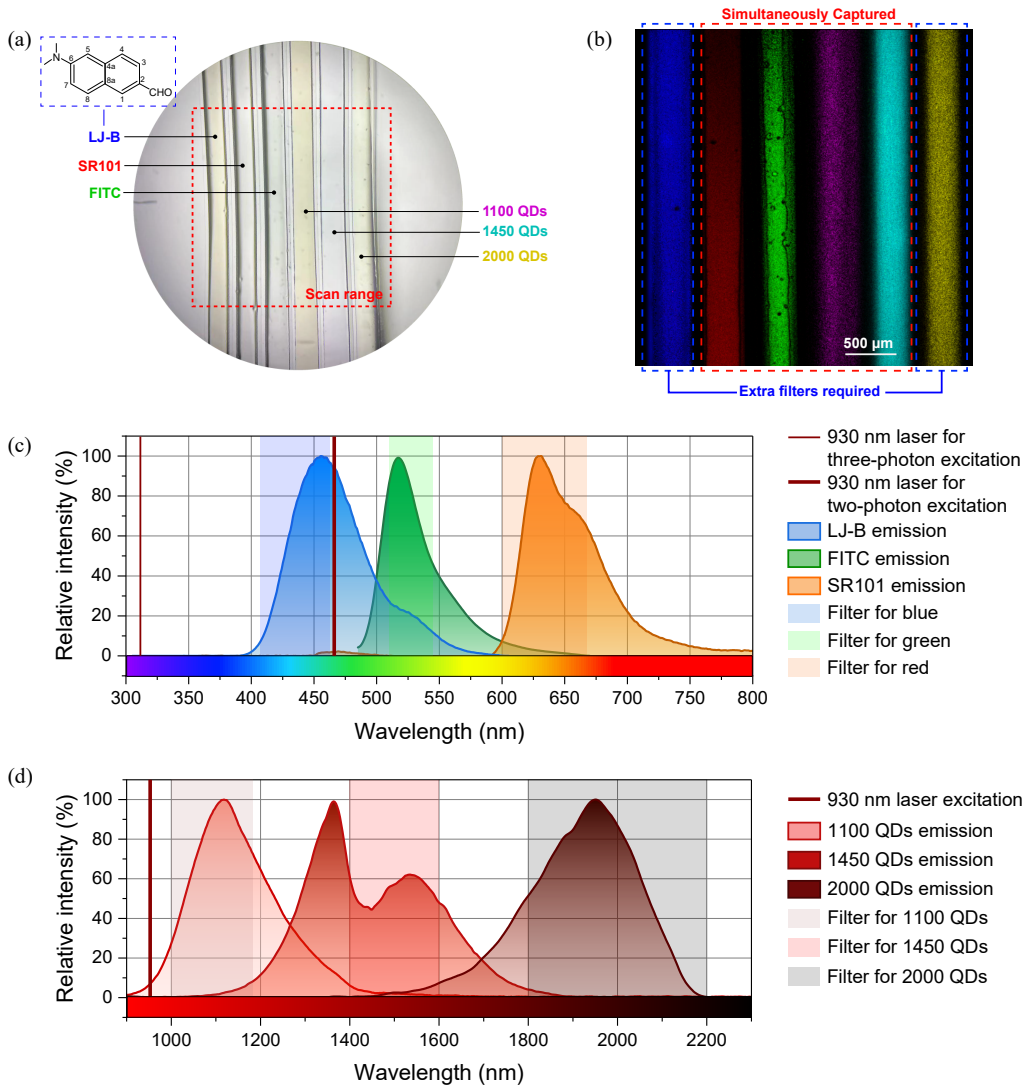

FIGURE 3. *In Vitro* Multi-channel microscopic imaging. (a) A bright-field microscopic image captured with a 5x objective lens, showcasing the six capillaries containing distinct fluorescent probes: LJ-B (molecular structure is showed in the inset), SR101, FITC, 1100 QDs, 1450 QDs and 2000 QDs. (b) A composite multi-channel fluorescence image demonstrating the simultaneous acquisition of fluorescence from the four centrally located capillaries. The capillaries positioned at the periphery of the field of view required the installation of supplementary filters for image acquisition, thus necessitating a sequential rather than simultaneous imaging process. (c) Fluorescence emission spectra of visible fluorescent probes, along with the designated spectral windows for each imaging channel. (d) Fluorescence emission spectra for NIR-II quantum dots, with the spectral windows specific to each imaging channel.

substantial depths. This laser was integrated into a commercial scanning microscope platform. The system is designed to achieve simultaneous multi-channel imaging by leveraging probes with distinct up-conversion and down-conversion fluorescence emission wavelengths, as depicted in Figure 6(a). A three-channel SNSPD was employed for the detection of NIR-II fluorescence signals, while two photomultiplier tubes (PMTs) sensitive to visible light were utilized for the detection of visible fluorescence, as detailed in the Methods section.

By integrating multiphoton fluorescence microscopy with NIR-II fluorescence confocal microscopy, a single 930 nm pulsed light source can be harnessed to concurrently excite both up-conversion multiphoton visible fluorescence and down-conversion single-photon NIR-II fluorescence. A dichroic mirror was used to spectrally separate the excited visible fluorescence from the NIR-II fluorescence. The implementation of a unified excitation light source within the multi-channel microscopic system ensures that all channels are uniformly excited at the exact same focal point, thereby eliminating discrepancies in depth-of-focus that may arise from the toggling of multiple excitation sources. By integrating fluorescent probes with distinct emission spectra, our system enables simultaneous multi-channel imaging. In this study, we utilized six distinct probes: LJ-B, FITC, SR101, 1100 QDs, 1450 QDs, and 2000 QDs (for detailed specifications, refer to the Methods section). They were encapsulated within

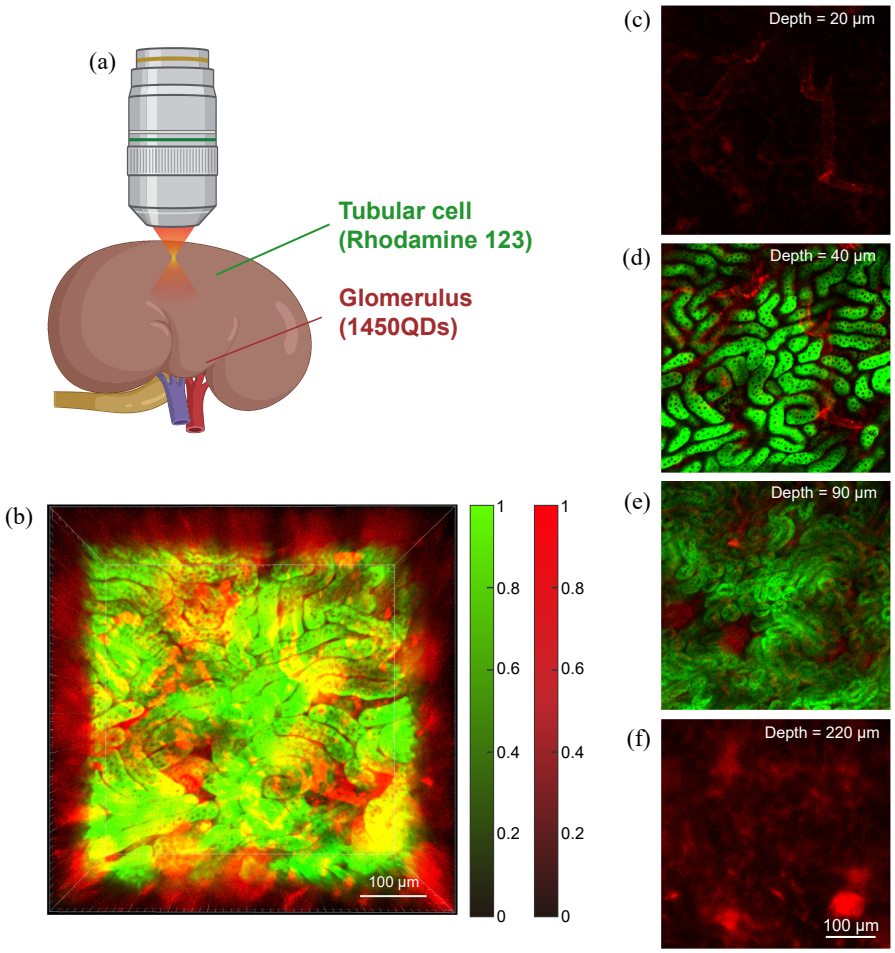

FIGURE 4. *In Vivo* Dual-channel microscopic imaging of mouse kidney. (a) Schematic representation of the imaging setup. Renal tubules are visualized in green following labeling with Rhodamine 123, while glomeruli and renal vessels are delineated in red after labeling with 1450 QDs. (b) Three-dimensional reconstruction of the dual-channel imaging of mouse kidney tissues. Scale Bar: 100 μm. (c)–(f) Dual-channel microscopic images captured at varying depths. Two-photon fluorescence imaging is executed up to a depth of approximately 100 μm, beyond which the signal fades. In contrast, the NIR fluorescence confocal channel sustains imaging capabilities, extending the observable depth to around 220 μm. Scale Bar: 100 μm.

capillary glass tubes separately for multichannel imaging, as illustrated in Figures 3(a), (b). The four capillaries positioned centrally within the field of view are capable of acquiring both their two-photon and NIR-II confocal fluorescence images concurrently. However, the capillary tubes situated at the extremities of the field of view, namely the far left and far right, necessitate a filter change to capture their images, precluding their simultaneous acquisition. Additionally, an analysis of the *in vitro* imaging intensity of capillaries was conducted, with each channel being quantified in isolation. Minimal inter-channel crosstalk was observed (Figure S6 in Supplementary Information). The SBR for each channel was notably high, surpassing 17. In the majority of cases, the SBRs were significantly higher, exceeding 70.

2.3. *In Vivo* Dual-Channel Microscopic Imaging of the Mouse Kidney

Utilizing the established multi-channel microscope system, we executed dual-channel imaging of mouse kidneys. 1450 QDs were employed for glomerular labeling, while Rhodamine 123 was selected for the visualization of cellular mitochondria, as depicted in Figure 4(a). Following the intravenous administration of the two fluorescent probes, Rhodamine 123 rapidly translocated into the kidney cells. Concurrently, 1450 QDs circulated through the vasculature, illuminating the glomeruli. At the superficial depths, the renal blood vessels were observable on the kidney's surface (Figure 4(c)). Upon increasing the imaging depth, the tubular architecture (green) of the kidney became distinctly discernible, with blood vessels (red) encircling this structure (Figure 4(d)). At a depth of approximately 90 μm, nearing the imaging depth threshold for the two-photon fluorescence channel, the glomeruli, visualized in the NIR-II channel (red), became discernible interspersed within the renal tubules of the green channel (Figure 4(e)). Upon progressive augmentation of the imaging depth, the signal from the two-photon fluorescence channel diminished and eventually became undetectable, while the NIR-II fluorescence channel maintained its signal, permitting imaging down to depths of up to 220 μm, as

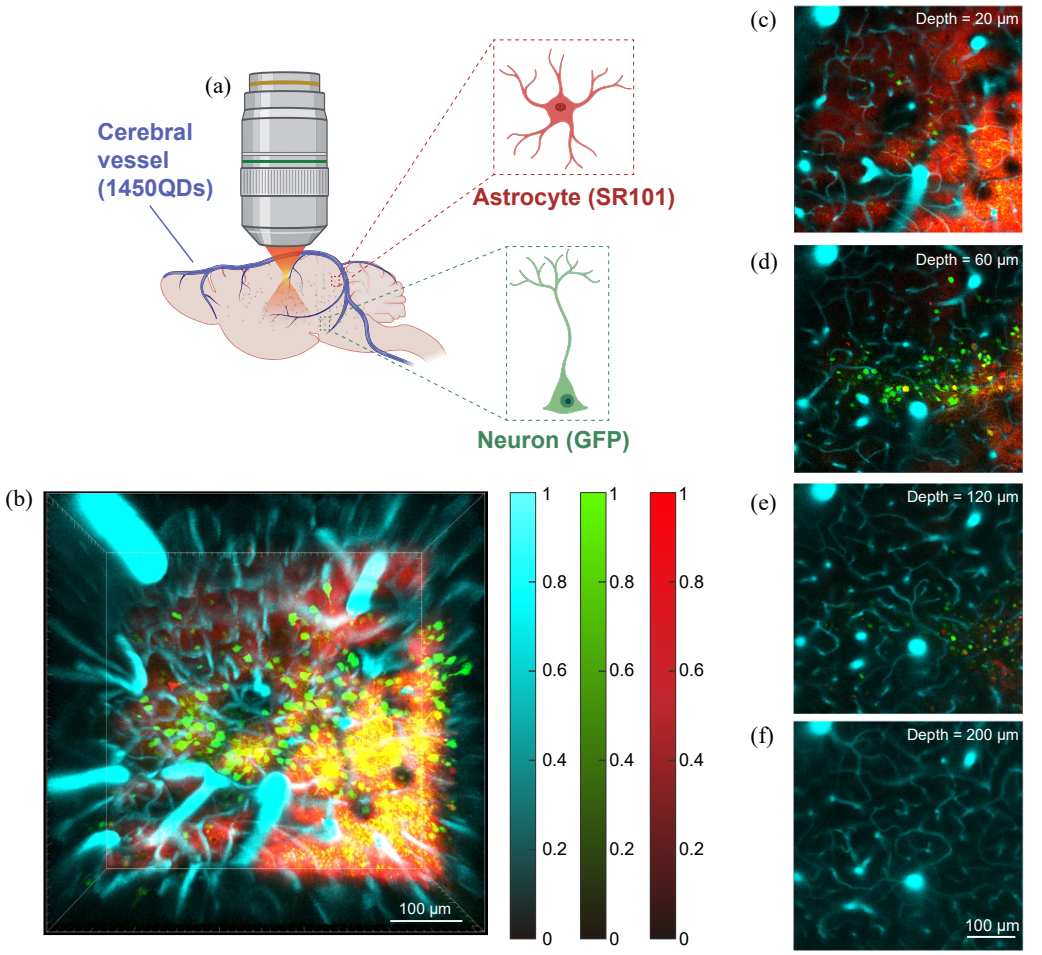

FIGURE 5. *In vivo* Three-channel microscopic imaging of mouse brain. (a) A schematic representation of the imaging setup. The red channel corresponds to astrocytes labeled with SR101, the green channel represents neurons labeled with GFP and the cyan channel depicts brain vasculature labeled with 1450 QDs. (b) A 3D reconstruction of the three-channel imaging of mouse brain, with a scale bar indicating 100 μm. (c)–(f) Three-channel microscopic images at varying depths are displayed. At a depth of 120 μm, neurons and astrocytes remain discernible, utilizing the effective signal captured by two-photon fluorescence microscopy as a depth reference. The imaging capability of NIR-II fluorescence confocal microscopy extends well beyond the depth range achievable with two-photon fluorescence microscopy. Scale bar: 100 μm.

illustrated in Figure 4(f). The 3D reconstructed image is shown as Figure 4(b). The system uses one excitation source for both NIR-II fluorescence confocal and two-photon fluorescence microscopies. NIR-II fluorescence confocal microscopy, using linear excitation, is effective, while two-photon fluorescence microscopy requires higher peak power density and precise focusing, limiting its deep tissue signal generation. The NIR-II channel records longer wavelength fluorescence, reducing scattering and enhancing tissue penetration compared to visible fluorescence. Thus, NIR-II fluorescence confocal microscopy achieves larger imaging depth than two-photon fluorescence microscopy when adopting the same excitation source.

The dwell time of the scanning system was set to 4 μs/pixel, and two imaging channels are acquired simultaneously.

2.4. *In Vivo* Three-Channel Microscopic Imaging of the Mouse Brain

Utilizing the multi-channel microscopic system, we conducted *in vivo* imaging of the mouse brain. Following craniotomy to expose the brain tissue, an imaging cranial window was established. Green fluorescent protein (GFP) was employed for the visualization of mouse neurons, while SR101 was used for the delineation of astrocytes, and blood vessels were highlighted using 1450 QDs, as depicted in Figure 5(a). SR101, when dissolved in water, was applied directly onto the brain tissue, allowing the dye to permeate the tissue and selectively label astrocytes. Post-staining, saline was meticulously used to eliminate any residual dye from the brain tissue surface, ensuring the clarity of the subsequent imaging process.

A substantial influx of SR101 into the cells results in the blood vessels exhibiting a negative contrast in the red two-photon fluorescence channel, which is accentuated at shallower imaging depths (Figure 5(c)). Neuronal signal intensity was

notably higher at an imaging depth of 60 μm, as depicted in Figure 5(d). The signal from green and red channel comparatively diminished at a depth of 120 μm, as illustrated in Figure 5(e). This phenomenon is potentially caused by incomplete removal of residual staining material. Vascular structures exhibiting negative contrast within the red two-photon fluorescence channel demonstrated a precise spatial correlation with those displaying positive contrast in the NIR-II fluorescence confocal channel. The imaging depth achievable with NIR-II confocal microscopy in brain tissue markedly surpassed that of two-photon fluorescence microscopy. We successfully accomplished three-channel microscopic imaging at a depth of approximately 200 μm, utilizing the visibility of structural features across all imaging channels as an indicator of effective imaging depth (Figures 5(b), (f)).

The dwell time of the scanning system was set to 4 μs/pixel, and three imaging channels are acquired simultaneously.

2.5. Assessing the Limitations of the 1400 nm Long-Pass Window in Imaging Scenarios

While our research has identified the 1400 nm LP window as offering distinct advantages in NIR-II fluorescence confocal microscopy, it is important to recognize that it is not universally applicable. The fluorescence intensity of probes emitting at wavelengths beyond 1400 nm must be sufficiently high to ensure effective imaging, particularly when the trailing edge of the fluorescence emission spectrum is employed for visualization. However, in cases where fluorescent probes have low brightness, the benefits of the 1400 nm LP window may be diminished. Therefore, the choice of the optimal imaging window should be guided by the specific characteristics of the fluorescent probes and the biological context under investigation.

In scenarios where the fluorescent probes exhibit high brightness across a broad spectrum, the 1400 nm LP window will likely remain more effective than the 1500 nm LP window. This superiority stems from the significant reduction of multiply scattered fluorescence photons within the 1400–1500 nm spectral band, which is attributable to the pronounced absorption of water in biological tissues. The absorption attenuates the scattered fluorescence photons, preventing them from entering the confocal pinhole and contributing to the imaging background.

2.6. The Application Potential of Multi-Channel Microscopic Imaging Systems in Biomedical Research

Multi-channel *in vivo* microscopic imaging transcends the conventional boundaries of biological observation. This advanced method not only facilitates the visualization of animal organs in their natural, living state but also provides a platform for in-depth, long-term monitoring of a diverse array of cellular components. By employing multiple imaging channels, researchers can simultaneously capture and analyze various cellular processes, such as cell division, migration, and interactions, within the complex microenvironment of living tissues. By employing coupling techniques to conjugate fluorescent probes with certain target molecules, the system can enable the tracking of various cell types and biomolecules, offering a more nuanced understanding of cellular behavior and physiological responses over time. The use of advanced imaging modalities, such as NIR-II fluorescence confocal microscopy, two-photon fluorescence microscopy, and intravital imaging, allows for high-resolution, three-dimensional imaging of cellular dynamics without the need for tissue excision or fixation. Furthermore, the integration of time-lapse imaging within this framework enables the study of dynamic cellular changes over extended periods, providing valuable insights into the temporal progression of biological processes. This is particularly relevant in the study of disease progression, where understanding the temporal dynamics of cellular alterations is crucial for developing effective therapeutic strategies.

In the future, integrating super-resolution techniques with multi-photon fluorescence and NIR-II fluorescence confocal microscopy can improve spatial resolution, enabling the simultaneous observation of intracellular dynamics and interactions, as well as tissue physiology. This multichannel microscopic imaging approach will enhance our understanding of cellular processes by enabling detailed analysis of molecular movements, signaling pathways, and cellular component interactions. These insights will be crucial for advancing medical research, drug mechanism elucidation, and the development of new therapeutic strategies.

3. METHODS AND MATERIALS

3.1. Fluorescence Probes

The dye LJ-B (molecule 6-(dimethylamino)-2-naphthaldehyde) was synthesized by our group, and the molecular structure is shown in Figure 3. FITC and Rhodamine 123 were purchased from FEIYUBIO, China. Sulforhodamine 101 (SR101) was purchased from XIMO, China. PbS/CdS quantum dots, exhibiting distinct fluorescence emission spectra, were synthesized and processed in-house. These quantum dots are designated as 1100 QDs and 1450 QDs, respectively, based on their emission peaks. Detailed methodologies of their synthesis, subsequent biocompatibility treatments, and cytotoxicity assessments are elaborated in our preceding publications [26–29]. HgTe quantum dots (2000 QDs) was kindly provided by Prof. Menglu Chen. The emission spectra of these quantum dots are illustrated in Figure 3(d).

3.2. Animal Preparation

All animal studies were conducted under the Guide for the Care and Use of Laboratory Animals, and the protocol was approved by the Medical Experimental Animal Care Commission of Zhejiang University (#ZJU20240719). Experimental animals were fed with clean water and standard laboratory chow. The housing area for experimental animals was maintained at 24°C with a 12-h day-night cycle.

For *in vivo* dual-channel microscopic imaging of kidney, rhodamine 123 was utilized for the specific staining of renal mitochondria. A solution of Rhodamine 123, prepared at a concentration of 1.5 mg/ml in physiological saline, was administered intravenously to mice following the induction of anesthe-

sia. Subsequently, a dispersion of 1450 quantum dots, at a concentration of 5 mg/ml in water, was injected into vein. To create a stable and temporary imaging window, a cover glass was applied to the lateral abdominal region of the anesthetized mouse and secured to an optical platform via a support column. This setup ensured that the kidney was maintained in a suitable position for subsequent imaging studies. The experimental protocol was conducted using C57 mice.

For *in vivo* three-channel microscopic imaging of brain, Thy1-GFP mice, both male and female, were sourced from the animal facility at Zhejiang University to conduct multi-channel microscopic imaging studies on the murine brain. Following a craniotomy procedure, an aqueous solution of sulforhodamine 101 (SR101) was topically applied to the exposed brain tissue within the cranial cavity. The solution was allowed to penetrate the tissue freely for a duration of approximately 15 minutes to ensure adequate staining. Subsequently, any surplus dye solution was meticulously removed from the tissue surface using a saline rinse to prevent interference with subsequent imaging. Once the imaging window was sealed to maintain sterility and stability, an aqueous dispersion of 1450 QDs prepared at a concentration of 6 mg/mL in a volume of 150 µL, was administered intravenously through the tail vein of the mouse.

3.3. High-Resolution Large-Depth NIR-II Confocal Microscopic Imaging of Mouse Brain

The NIR-II fluorescence confocal microscope used for imaging deep brain tissues in living mice is showed in Figure S4 in Supplementary Information. The 1177 nm CW or 930 nm femtosecond laser beam is directed through a flip-flop mirror, traversing into the microscope. A Dichroic Cage Cube (DM cube, MCM1S-A, LBTEK, China) houses an 1180 nm short-pass dichroic mirror (DM10-1180SP, LBTEK, China). The excitation beam, after passing through this dichroic mirror, proceeds into the microscope, traversing the galvanometric mirrors, scan lens, tube lens, and ultimately the microscope objective (XLPLN25XWMP2-SP, Olympus, Japan) to achieve focal convergence within the target tissue. The emitted fluorescence is retro-reflected by the short-pass dichroic mirror in the Dichroic Cage Cube, passing through an interchangeable long-pass filter (EFLH1300, EFLH1400, or EFLH1500, Thorlabs, USA), before being collimated by a Reflective collimator (RC02APC-P01, Thorlabs, USA) and coupled into a single-mode fiber (SM fiber in Figure S4 in Supplementary Information, MCSFP-1550-SMF-FA, MC Fiber Optics, China). The signal is then transmitted via the fiber to an SNSPD (P-SPD-nS, Photec, China).

The cerebral cortex of the mouse was accessed through a surgical procedure, and a cranial window was meticulously fashioned to facilitate subsequent imaging studies. The mice were intravenously injected with a dispersion of 1450 QDs at a concentration of 5 mg/mL, with a total volume of 150 µL. The quantum dots were excited using the 1177 nm CW laser, which was operated at a maximum power of 26 mW before the objective, or the 930 nm femtosecond laser, operated at a maximum power of 20 mW before the objective. The NIR-II confocal imaging system was configured with a scanning dwell time of 4 µs/pixel.

3.4. Multi-Channel Imaging System Integrating Multiphoton Fluorescence and NIR-II Fluorescence Confocal Microscopy

In this work, a multi-channel microscope system was built based on a laser scanning microscope (FVMPE-RS, Olympus, Japan), as shown in Figure 6. A 930 nm femtosecond laser beam (YLMO930, MenloSystems) passes through an optical path climbing system (OBS-505, LBTEK, China) and transmits through a Dichroic Cage Cube (DM cube1, MCM1S-A, LBTEK, China). A 1000 nm short-pass dichroic mirror (DM10-1000SP, LBTEK, China) is installed in the Cube. The laser light enters the scanning microscope and passes through the galvanometers, scan lens, tube lens, and focuses on the target tissue through the microscope objective (XLPLN25XWMP2-SP, Olympus, Japan) in turn. The objective is immersed with heavy water (A45671, Beijing Wokai Biotechnology Co., China). The fluorescence is excited and escapes from the tissue, and after passing through the objective lens, the multiphoton excited visible fluorescence is reflected on changeable dichroic mirrors (DM1, DMLP900R, Thorlabs, USA; DMLP670R, Thorlabs, USA) into changeable fluorescence beamsplitters, and ultimately reaches the two visible-sensitive PMTs. To discern between red and green emissions, a 580 nm long-pass dichroic mirror (DMGR in Figure 6(a), FV30-FGR, Olympus, Japan) is utilized, with the red fluorescence channel defined as 600–645 nm and the green fluorescence channel as 510–540 nm. Additionally, a 485 nm long-pass dichroic mirror (DMVG in Figure 6(d), FV30-FVG, Olympus, Japan) is applied to differentiate between blue and green lights, with the blue fluorescence channel ranging from 410 to 460 nm.

The NIR-II fluorescence sequentially transmits through a dichroic mirror 1 (DM1), a tube lens, a scan lens, and galvanometric mirrors before being directed towards a Dichroic Cage Cube (referred to as DM cube 1). This cube reflects the light and divides it into two distinct beams. A second Dichroic Cage Cube (DM cube 2, MCM1S-A, LBTEK, China) further bifurcates the beams. This cube is equipped with a 1180 nm long-pass dichroic mirror (DMLP1180R, Thorlabs, USA), which reflects fluorescence wavelengths shorter than 1180 nm. This reflected light then traverses a 1000 nm long-pass filter (FELH1000, Thorlabs, USA) and is subsequently focused by a reflective collimator (RC1, RC02APC-P01, Thorlabs, USA) into a single-mode fiber (SM fiber 1 in Figure 6(b), MCSFP-1064-H1-SMF-FA, MC Fiber Optics, China). The light then transmits through this fiber to reach the SNSPD (P-SPD-nS, Photec, China) in channel 1 (CH1 in Figure 6(e)). Fluorescence with wavelengths exceeding 1200 nm is transmitted through the second dichroic cage cube (DM cube 2), where it is further filtered by a 1400 nm long-pass filter (EFLH1400, Thorlabs, USA) to ensure the passage of only longer wavelengths. Subsequently, the filtered light is focused into a replaceable single-mode fiber (SM fiber2 in Figures 6(a), (c), RC02APC-P01, Thorlabs, USA) by a second reflective collimator (RC2 in Figures 6(a), (c), Thorlabs, USA). For the detection of fluores-

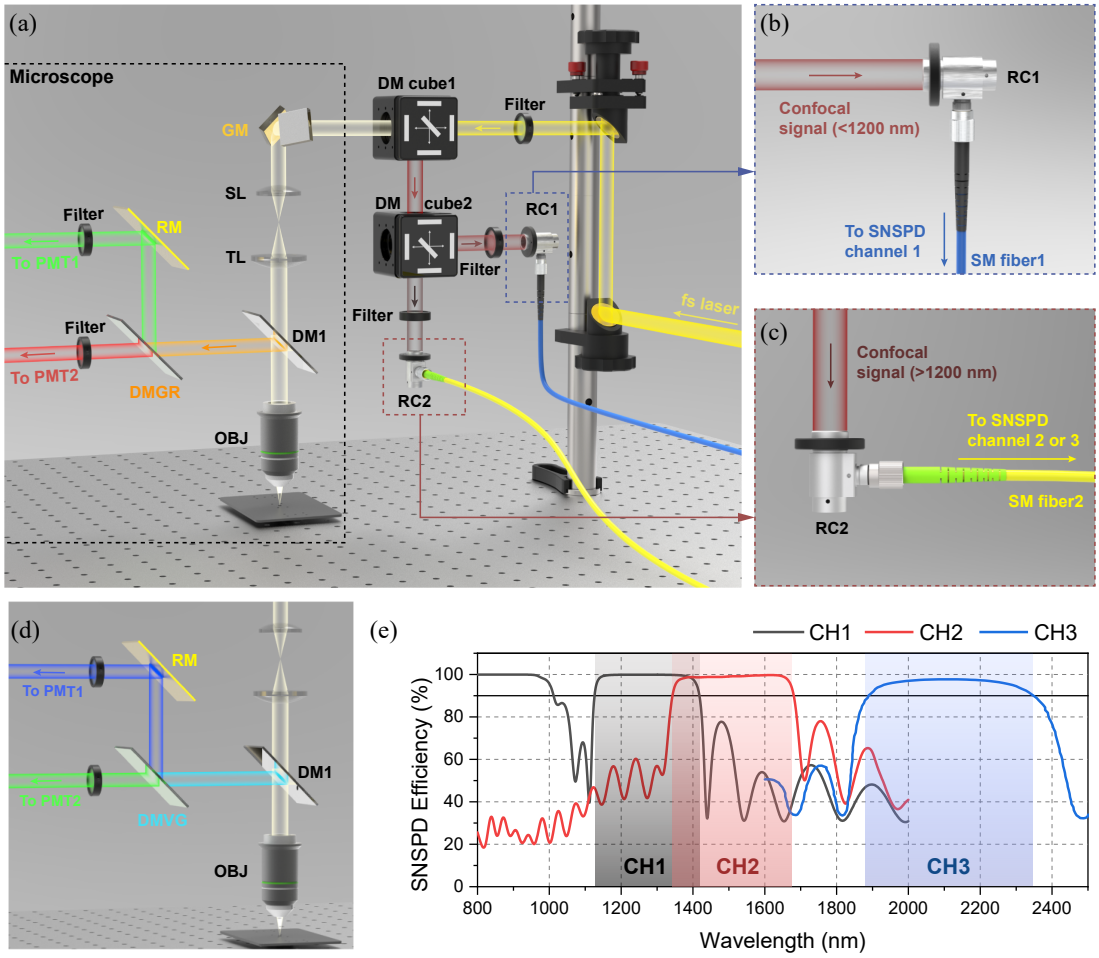

FIGURE 6. Schematic representation of the multichannel microscopic imaging system (a) The optical pathway within the multi-channel microscopic imaging system. Abbreviations: DM (Dichroic Mirror), GM (Galvanometers), SL (Scan Lens), TL (Tube Lens), RC (Reflective Collimator), OBJ (Objective Lens), RM (Reflecting Mirror), PMT (Photomultiplier Tube). (b) Signal light with wavelengths below 1200 nm is directed into the single-mode fiber by the reflective collimator RC1, subsequently being conveyed to channel 1 of SNSPD. (c) Signal light with wavelengths exceeding 1200 nm is coupled into the single-mode fiber by the reflective collimator RC2, and is then routed to either channel 2 or channel 3 of SNSPD. (d) The process of replacing the visible dichroic mirror (DMVG), enabling the spectral separation and detection of blue and green fluorescence. (e) The three detection channels of the SNSPD along with their respective detection efficiency spectra.

cence within the range of 1200–1700 nm, a single-mode fiber (MCSFP-1550-S2-SMF-28e, MC Fiber Optics, China) with a center wavelength of 1550 nm is utilized. This fiber is connected to the second detection channel of SNSPD (CH2 in Figure 6(e)). To receive fluorescence in the range of 1800–2200 nm, a single-mode fiber (MCSFP-1950-FA, MC Fiber Optics, China) with a center wavelength of 1950 nm is employed. This fiber is connected to the third detection channel of the SNSPD (CH3 in Figure 6(e)), thereby facilitating the comprehensive detection of fluorescence across the specified wavelength ranges.

Our system, which is constructed on a commercial microscope (FVMPE-RS, Olympus, Japan), is equipped with two PMTs sensitive to visible light, thereby enabling the concurrent detection of only two visible channels. In a similar vein, the infrared detection channel is limited to two SNSPDs, which restricts its capacity to detect only two kinds of signals at a time. The system is designed to detect four channels simultaneously, the green channel is consistently observable. In contrast, the blue and red channels are subject to a mutual exclusivity, allowing for the detection of only one at any given time due to the need to replace additional filters and optical fibers. This constraint is also applicable to SNSPD, where channels CH2 and CH3 are not compatible for concurrent operation. The microscopic imaging system utilized a shared scanning galvanometer system across all channels. The dwell time of the scanning system was optimized to prioritize channels equipped with SNSPD to ensure proper exposure. Subsequently, the bias voltage of PMTs was adjusted to guarantee normal exposure for the visible channels as well.

3.5. *In Vitro* Multi-Channel Microscopic Imaging

In this work, the microscopic imaging system has been engineered to integrate up- and down-conversion fluorescence detection, thereby facilitating the simultaneous imaging of up to

4 distinct channels, as depicted in Figure 3(b). This advanced system design allows for an analysis of multiple fluorescent probes within a single imaging session. For *in vitro* imaging, capillary glass tubes with an inner diameter of 0.1 mm were employed. The visible fluorescent probes utilized for multiphoton excitation in this research encompass LJ-B, FITC, and SR101, with their respective fluorescence emission spectra illustrated in Figure 3(c). In the realm of NIR-II fluorescence, quantum dots were incorporated, specifically 1100 QDs, 1450 QDs, and 2000 QDs, and their spectral profiles are presented in Figure 3(d). To achieve imaging of these six diverse fluorescent probes within a unified field of view, a $5\times$ microscope objective (LMPlanFL $5\times$ BD, Olympus, Japan) was utilized. This objective provided the necessary magnification and clarity for the detection and analysis of the fluorescent signals. The corresponding bright field images, which serve as a reference for the fluorescent imaging, are displayed in Figure 3(a). The imaging system is capable of acquiring four-channel images in a single session. In the configuration exemplified, the system was equipped to capture two channels of visible light fluorescence — SR101 for the red spectrum (600–645 nm) and FITC for the green spectrum (510–540 nm) — as well as two channels of NIR-II fluorescence — 1100 QDs for the range of 1000–1180 nm and 1450 QDs for the range of 1400–1600 nm.

4. CONCLUSION

In our study, we evaluated NIR-II fluorescence confocal microscopy's imaging quality across different fluorescence wavelengths. We found that wavelengths above 1400 nm provided superior SBR. Using 1177 nm excitation, we achieved deep-tissue imaging of the mouse brain to a depth of 1.2 mm, and with 930 nm femtosecond laser excitation, we imaged to 1.1 mm. Our system resolved blood vessels as small as 3.53 µm at maximum depth.

The 930 nm femtosecond laser's multiphoton excitation capability was leveraged to enhance microscopy's depth penetration. We developed a multi-channel imaging system using this laser, combining multiphoton fluorescence and NIR-II confocal imaging. This system captured images from various fluorescent probes, offering comprehensive sample analysis. An in vitro six-channel experiment demonstrated the system's emission detection capabilities with wavelengths from visible to near infrared, covering 400–800 nm, 1000–1700 nm, and 1900–2300 nm.

The system was used for *in vivo* multi-channel imaging of the mouse brain and kidney, achieving three-channel imaging at 200 µm depth. It visualized blood vessels, neurons, and astrocytes in the brain, and selectively labeled renal structures in the kidney, providing morphological assessments. These experiments showcased the system's deep tissue penetration and high-resolution imaging, which will be a valuable tool for studying cellular interactions and tissue organization *in vivo*.

ACKNOWLEDGEMENT

This work was supported by the National Key R&D Program of China (2022YFB3206000), Dr. Li Dak Sum & Yip Yio Chin Development Fund for Regenerative Medicine, Zhejiang University, the Fundamental Research Fund for the Central Universities (K20220220), and the National Natural Science Foundation of China (61975172).

REFERENCES

[1] Wang, F., Y. Zhong, O. Bruns, Y. Liang, and H. Dai, "In vivo NIR-II fluorescence imaging for biology and medicine," *Nature Photonics*, 535–547, 2024.

[2] Ramani, R. S., I. Tan, L. Bussau, C. M. Angel, M. McCullough, and T. Yap, "Confocal microscopy in oral cancer and oral potentially malignant disorders: A systematic review," *Oral Diseases*, Vol. 29, No. 8, 3003–3015, 2023.

[3] Teo, A. W. J., H. Mansoor, N. Sim, M. T.-Y. Lin, and Y.-C. Liu, "In vivo confocal microscopy evaluation in patients with keratoconus," *Journal of Clinical Medicine*, Vol. 11, No. 2, 393, 2022.

[4] Hong, G., S. Diao, J. Chang, A. L. Antaris, C. Chen, B. Zhang, S. Zhao, D. N. Atochin, P. L. Huang, K. I. Andreasson, C. J. Kuo, and H. Dai, "Through-skull fluorescence imaging of the brain in a new near-infrared window," *Nature Photonics*, Vol. 8, No. 9, 723–730, 2014.

[5] Welsher, K., Z. Liu, S. P. Sherlock, J. T. Robinson, Z. Chen, D. Daranciang, and H. Dai, "A route to brightly fluorescent carbon nanotubes for near-infrared imaging in mice," *Nature Nanotechnology*, Vol. 4, No. 11, 773–780, 2009.

[6] Feng, Z., T. Tang, T. Wu, X. Yu, Y. Zhang, M. Wang, J. Zheng, Y. Ying, S. Chen, J. Zhou, and e. al., "Perfecting and extending the near-infrared imaging window," *Light: Science & Applications*, Vol. 10, No. 1, 197, 2021.

[7] Yong, K.-T., J. Qian, I. Roy, H. H. Lee, E. J. Bergey, K. M. Tramposch, S. He, M. T. Swihart, A. Maitra, and P. N. Prasad, "Quantum rod bioconjugates as targeted probes for confocal and two-photon fluorescence imaging of cancer cells," *Nano Letters*, Vol. 7, No. 3, 761–765, 2007.

[8] Chu, L., S. Wang, K. Li, W. Xi, X. Zhao, and J. Qian, "Biocompatible near-infrared fluorescent nanoparticles for macro and microscopic in vivo functional bioimaging," *Biomedical Optics Express*, Vol. 5, No. 11, 4076–4088, 2014.

[9] Sun, C., Y. Wang, H. Zhang, and J. Qian, "Near-infrared laser scanning confocal microscopy and its application in bioimaging," *Optical and Quantum Electronics*, Vol. 50, 1–9, 2018.

[10] Alifu, N., A. Zebibula, J. Qi, H. Zhang, C. Sun, X. Yu, D. Xue, J. W. Y. Lam, G. Li, J. Qian, and B. Z. Tang, "Single-molecular near-infrared-ii theranostic systems: Ultrastable aggregation-induced emission nanoparticles for long-term tracing and efficient photothermal therapy," *ACS Nano*, Vol. 12, No. 11, 11 282–11 293, 2018.

[11] Yu, W., B. Guo, H. Zhang, J. Zhou, X. Yu, L. Zhu, D. Xue, W. Liu, X. Sun, and J. Qian, "NIR-II fluorescence in vivo confocal microscopy with aggregation-induced emission dots," *Science Bulletin*, Vol. 64, No. 6, 410–416, 2019.

[12] He, M., D. Wu, Y. Zhang, X. Fan, S. Zhuang, W. Yang, H. Lin, and J. Qian, "Protein-enhanced NIR-IIb emission of indocyanine green for functional bioimaging," *ACS Applied Bio Materials*, Vol. 3, No. 12, 9126–9134, 2020.

[13] Zhou, J., T. Wu, R. Chen, L. Zhu, H. Zhang, Y. Li, L. Chen, and J. Qian, "Self-confocal NIR-II fluorescence microscopy for multifunctional in vivo imaging," *Journal of Innovative Optical Health Sciences*, Vol. 17, No. 1, 2350025, 2024.

[14] Xia, F., M. Gevers, A. Fognini, A. T. Mok, B. Li, N. Akbari, I. E. Zadeh, J. Qin-Dregely, and C. Xu, "Short-wave infrared

confocal fluorescence imaging of deep mouse brain with a superconducting nanowire single-photon detector," *ACS Photonics*, Vol. 8, No. 9, 2800–2810, 2021.

[15] Wang, F., F. Ren, Z. Ma, L. Qu, R. Gourgues, C. Xu, A. Baghdasaryan, J. Li, I. E. Zadeh, J. W. N. Los, A. Fognini, J. Qin-Dregely, and H. Dai, "In vivo non-invasive confocal fluorescence imaging beyond 1,700 nm using superconducting nanowire single-photon detectors," *Nature Nanotechnology*, Vol. 17, No. 6, 653–660, 2022.

[16] Wu, T., Y. Wang, H. Lin, and J. Qian, "A pervasive approach for determining the optimal tissue windows for near-infrared fluorescence imaging," *Laser & Photonics Reviews*, 2400628, 2024.

[17] Bandi, V. G., M. P. Luciano, M. Saccomano, N. L. Patel, T. S. Bischof, J. G. P. Lingg, P. T. Tsrunchev, M. N. Nix, B. Ruehle, C. Sanders, and e. al., "Targeted multicolor in vivo imaging over 1,000 nm enabled by nonamethine cyanines," *Nature Methods*, Vol. 19, No. 3, 353–358, 2022.

[18] Cosco, E. D., B. A. Arús, A. L. Spearman, T. L. Atallah, I. Lim, O. S. Leland, J. R. Caram, T. S. Bischof, O. T. Bruns, and E. M. Sletten, "Bright chromenylium polymethine dyes enable fast, four-color in vivo imaging with shortwave infrared detection," *Journal of the American Chemical Society*, Vol. 143, No. 18, 6836–6846, 2021.

[19] Cosco, E. D., A. L. Spearman, S. Ramakrishnan, J. G. P. Lingg, M. Saccomano, M. Pengshung, B. A. Arús, K. C. Y. Wong, S. Glasl, V. Ntziachristos, M. Warmer, R. R. McLaughlin, O. T. Bruns, and E. M. Sletten, "Shortwave infrared polymethine fluorophores matched to excitation lasers enable non-invasive, multicolour in vivo imaging in real time," *Nature Chemistry*, Vol. 12, No. 12, 1123–1130, 2020.

[20] He, Y., S. Wang, P. Yu, K. Yan, J. Ming, C. Yao, Z. He, A. M. El-Toni, A. Khan, X. Zhu, C. Sun, Z. Lei, and F. Zhang, "NIR-II cell endocytosis-activated fluorescent probes for in vivo high-contrast bioimaging diagnostics," *Chemical Science*, Vol. 12, No. 31, 10 474–10 482, 2021.

[21] Lu, L., B. Li, S. Ding, Y. Fan, S. Wang, C. Sun, M. Zhao, C.-X. Zhao, and F. Zhang, "NIR-II bioluminescence for in vivo high contrast imaging and in situ ATP-mediated metastases tracing," *Nature Communications*, Vol. 11, No. 1, 4192, 2020.

[22] Yang, Y., Y. Xie, and F. Zhang, "Second near-infrared window fluorescence nanoprobes for deep-tissue in vivo multiplexed bioimaging," *Advanced Drug Delivery Reviews*, Vol. 193, 114697, 2023.

[23] Yao, C., Y. Chen, M. Zhao, S. Wang, B. Wu, Y. Yang, D. Yin, P. Yu, H. Zhang, and F. Zhang, "A bright, renal-clearable NIR-II brush macromolecular probe with long blood circulation time for kidney disease bioimaging," *Angewandte Chemie*, Vol. 134, No. 5, e202114273, 2022.

[24] Gerdes, H.-H. and C. Kaether, "Green fluorescent protein: Applications in cell biology," *FEBS Letters*, Vol. 389, No. 1, 44–47, 1996.

[25] Gallo, E., "Fluorogen-activating proteins: Next-generation fluorescence probes for biological research," *Bioconjugate Chemistry*, Vol. 31, No. 1, 16–27, 2020.

[26] Huang, B., J. Hu, H. Li, M.-Y. Luo, S. Chen, M. Zhang, Z.-J. Sun, and R. Cui, "Near-infrared IIb emitting nanoprobe for high-resolution real-time imaging-guided photothermal therapy triggering enhanced anti-tumor immunity," *ACS Applied Bio Materials*, Vol. 3, No. 3, 1636–1645, 2020.

[27] Li, H., M. Wang, B. Huang, S.-W. Zhu, J.-J. Zhou, D.-R. Chen, R. Cui, M. Zhang, and Z.-J. Sun, "Theranostic near-infrared-IIb emitting nanoprobes for promoting immunogenic radiotherapy and abscopal effects against cancer metastasis," *Nature Communications*, Vol. 12, No. 1, 7149, 2021.

[28] Yu, G.-T., M.-Y. Luo, H. Li, S. Chen, B. Huang, Z.-J. Sun, R. Cui, and M. Zhang, "Molecular targeting nanoprobes with non-overlap emission in the second near-infrared window for in vivo two-color colocalization of immune cells," *ACS Nano*, Vol. 13, No. 11, 12 830–12 839, 2019.

[29] Zhang, M., J. Yue, R. Cui, Z. Ma, H. Wan, F. Wang, S. Zhu, Y. Zhou, Y. Kuang, Y. Zhong, D.-W. Pang, and H. Dai, "Bright quantum dots emitting at □1,600 nm in the NIR-IIb window for deep tissue fluorescence imaging," *Proceedings of the National Academy of Sciences*, Vol. 115, No. 26, 6590–6595, 2018.